INTERNATIONAL JOURNAL OF COMMUNICATION SYSTEMS
Int. J. Commun. Syst. 2014; **27**:2997–3012
Published online 6 March 2013 in Wiley Online Library (wileyonlinelibrary.com). DOI: 10.1002/dac.2521

Multiple Rayleigh fading channels modeling based on sum-of-sinusoids model

Yu Gan*,† and You Wu

Schaefer School of Engineering & Science, Stevens Institute of Technology, Hoboken, NJ 07030, USA

SUMMARY

Assessing the performance of communication system is critical in system design in mobile communication study. Numerous methodologies have been employed to facilitate the assessment, amongst which generation of multiple fading channels is widely used and thus of great interest to us. Specifically, multiple Rayleigh fading channels are extensively utilized in simulation of the following: MIMO channels, amplify-and-forward fading channels, frequency-selective channels, etc. The existing model to generate Rayleigh fading channels is the sum of sinusoids (SOS). However, the SOS model is flawed, as it sometimes generates impure correlated channels. That is, a small fraction of correlated channels are generated when we anticipate uncorrelated or vice versa. In this paper, on the basis of the concept of SOS, we introduce a new computational model to generate Rayleigh channels that completely match our anticipation—fully uncorrelated or fully correlated channels. Additionally, we also propose a design method to reduce the number of sinusoids, thus we achieve reduced computational cost of the system. Simulation results and comparison analysis indicate that, with reduced computational cost, our method is able to produce pure Rayleigh fading channels—100% uncorrelated or the opposite. Copyright © 2013 John Wiley & Sons, Ltd.

Received 9 July 2012; Revised 13 January 2013; Accepted 23 January 2013

KEY WORDS: mobile communications; Rayleigh process; SOS model; multiple fading channels

1. INTRODUCTION

Mobile communication technology experiences unprecedented development in recent decades, resulting in largely advanced performance of communication system. Various research have been carried out to assess and improve the performance of communication. Multiple Rayleigh fading channels haven been frequently utilized in assessing performance of communication system [1]. In many scenarios (e.g., wideband fading channels, MIMO channels, and diversity-combined fading channels, etc.) [2–4], an accurate Rayleigh fading channels generator enables assessment of the system in an efficient manner, especially when large scale field trial measurements are not available because of its high cost and non-reproducibility [5].

Multiple Rayleigh fading channels generator with high accuracy and efficiency, however, remains elusive. In the past decades, large quantity of different computational models, including deterministic, ergodic stochastic and non-ergodic stochastic process, have been investigated to generate multiple channels. A majority of previously proposed methods are based on the sum-of-sinusoid (SOS) model, which was initially discussed in [6, 7] and further developed in [8]. The most well-known SOS model is the Jakes' model [9], in which computational method was proposed to calculate parameters. Pop and Beaulieu suggested applying additional random phases to the Jakes' model, and they also discussed the properties of this model in [10]. Y. X. Li *et al.* in [11] modified Jakes'

*Correspondence to: Yu Gan, Schaefer School of Engineering & Science, Stevens Institute of Technology, Hoboken, NJ 07030, USA.
†E-mail: ygan@stevens.edu

model by using asymmetrical arrival angle arrangement and selecting incident wave phases. These studies offering diversity in system implementation, however, suffer the disadvantage of failing to achieve a good approximation of anticipated waveforms. Then, it was proven in [12] that the cross-correlation function (CCF) in Jakes' model is non-zero. To solve the non-zero problem of CCF, there has been a renewed interest in statistical models, which involves the uses of random phases and Doppler frequencies [13–18]. Because of the introduction of random Doppler frequencies, the simulation process becomes non-ergodic. Resultantly, the performance of auto-correlation function (ACF) is not sufficiently close to the reference ACF. Distinct from the stochastic model [19], the deterministic model does not share the same drawbacks of CCF and ACF. In [20], model of exact Doppler spread (MEDS) was proposed to generate multiple uncorrelated fading channels. The MEDS model, a deterministic model and proved later in [12] to be a quasi-optimal approximation of ACF, has good performance of the first and the second order statistics. Because the selection of Doppler frequencies is unique when the number of sinusoids is determined, a large number of sinusoids have to be deployed when the number of channels increases. In [21], modifications are made to keep the uncorrelatedness without increasing the number of sinusoids. But authors in [22] using methods in [21] showed that the multiple paths decorrelate very slowly; thus, they proposed a generalized method of exact Doppler spread (GMEDS_q) that represents a class of parameter computation methods to model multiple uncorrelated Rayleigh fading channels. Two special cases of GMEDS_q, where $q = 1$ or 2, were discussed in detail to generate a large number of multiple uncorrelated Rayleigh fading channels. Authors in [23] introduced MEDS with set partitioning (MEDS-SP) to simulate a single trial of Rayleigh fading waveform. Gan and Xu [24] analyzed an issue when applying the GMEDS_q and focused on the generation of uncorrelated fading channels. Gutierrez *et al*., [25] presented a new design of ergodic simulator for multiple uncorrelated Rayleigh fading channel. Being different from the topics we discuss in this paper, Gutierrez's paper merely focused on the uncorrelated case under scatter condition. Besides the simulation of channel modeling, [26, 27] and [28] demonstrated the feasibility of applying the fading channel model in hardware implementation (e.g., field programmable gate array, digital signal processor).

In this paper, we first analyze the GMEDS_q in [22] by discussing a pitfall of existing methods; then, we introduce a new parameter computational method to overcome the pitfall. In particular, we propose a half-ring model to illustrate the working mechanism of our proposed method. Additionally, we employ the concept of set partition to efficiently generate multiple uncorrelated fading channels. We discuss the feasibility and advantage of the new method. Next, we apply our new method to generate multiple correlated fading channels. Finally, we present simulation results that confirm the high accuracy and efficiency of our new method.

Specifically, we make the following contributions.

- Because uncorrelated channels are mostly needed in system assessment, we first propose an accurate and efficient model to generate multiple uncorrelated Rayleigh fading channels. Specifically, we propose a parameter computational method and a system design method. We discuss in detail to show how our model generates channels that are fully uncorrelated and how to reduce the computational complexity.
- Considering that correlated channels are sometimes needed, we then extend our design on how to generate multiple correlated channels. On the basis of our model initially designed to generate uncorrelated channels, we apply a linear transform in our model so that we can also generate correlated channels. We demonstrate that, with known channel parameters, such as channel Doppler spread, maximum Doppler offset, time delay between the arrival of different envelopes, our model can also generate multiple correlated Rayleigh fading channels in an efficient manner.
- We perform simulation studies in the following aspects: correlation statistics, error analysis, complexity and envelope of waveforms. We compare our model with the reference model of Rayleigh process and also with the existing models. Experimental results demonstrate the high accuracy and effectiveness of our model.

The rest of this paper is organized as follows. Section 2 introduces the reference model of Rayleigh process and the principle of deterministic SOS model. In Section 3, we present our new parameter

DOI: 10.1002/dac

computational method. In Section 4, we propose our system design method. Section 5 discusses how to generate correlated fading channels. The performance of our model is evaluated in Section 6. At last, Section 7 concludes this paper.

2. THE SUM OF SINUSOIDS MODEL

2.1. Reference model

Rayleigh process is a strict sense stationary process and is the envelope of a zero-mean complex Gaussian random process. Here, we first focus on generating L Rayleigh fading channels. For the lth ($l \leqslant L$) Rayleigh process, the reference model can be expressed as

$$\zeta_l(t) = |\mu_l(t)| = |\mu_{1,l}(t) + j\,\mu_{2,l}(t)| \tag{1}$$

where $j = \sqrt{-1}$, $\mu_{1,l}(t)$ and $\mu_{2,l}(t)$ are uncorrelated real Gaussian random processes with variance σ_0^2.

For a Rayleigh process $\zeta_l(t)$, the PDF p_{ζ_l} follows:

$$p_{\zeta_l}(x) = \frac{x}{\sigma_0^2}\exp\left(-\frac{x^2}{2\sigma_0^2}\right) \quad x \geqslant 0 \tag{2}$$

For multiple uncorrelated Rayleigh fading channels, we investigate the auto-correlation and CCFs of the reference model. Under the assumption of two-dimensional isotropic scatter, the reference model is determined by the following [10, 29].

$$r_{\mu_{i,l}\mu_{i,l}}(\tau) = E\{\mu_{i,l}(t)\mu_{i,l}(t)\} = J_0(2\pi f_{\max}\tau) \tag{3}$$

$$r_{\mu_{i,l}\mu_{k,l}}(\tau) = E\{\mu_{i,l}(t)\mu_{k,l}(t)\} = 0, \quad i \neq k \tag{4}$$

$$r_{\mu_l\mu_l}(\tau) = E\{\mu_l(t)\mu_l(t)\} = J_0(2\pi f_{\max}\tau) \tag{5}$$

$$r_{\mu_l\mu_\lambda}(\tau) = E\{\mu_l(t)\mu_\lambda(t)\} = 0 \tag{6}$$

where $i = 1, 2$ and $l, \lambda = 1, 2, ..., L$ with $l \neq \lambda$. $J_0(\cdot)$ is the zeroth-order Bessel function of the first kind. These equations guarantee the uncorrelatedness among multiple Rayleigh channels. We expect to build a model that can produce L Rayleigh processes with precise approximation to (3)–(6).

2.2. The sum of sinusoids model

The principle of the SOS method is based on the central limit theorem. Using this theorem, we know that a Gaussian random process can be approximated closely by forming summation of series of properly selected sinusoids. In particular, the process can be expressed as:

$$\tilde{\zeta}_l(t) = |\tilde{\mu}_l(t)| = |\tilde{\mu}_{1,l}(t) + j\,\tilde{\mu}_{2,l}(t)| \tag{7}$$

Here,

$$\tilde{\mu}_{i,l}(t) = \sum_{n=1}^{N_{i,l}} c_{i,n,l}\cos(2\pi f_{i,n,l}t + \theta_{i,n,l}), i = 1, 2 \tag{8}$$

where $N_{i,l}$ denotes the number of sinusoids; real valued $c_{i,n,l}$, $f_{i,n,l}$ and $\theta_{i,n,l}$ are Doppler coefficients, discrete Doppler frequencies and Doppler phase, respectively. It is known that $N_{i,l} \to +\infty$, $\tilde{\mu}_{i,l}(t)$ follows Gaussian distribution at any instant of t. Thus, $\tilde{\zeta}_l(t)$ is a Rayleigh process. Many methods can be used to calculate the value of $c_{i,n,l}$, $f_{i,n,l}$ and $\theta_{i,n,l}$. In deterministic model, $c_{i,n,l}$ and $f_{i,n,l}$ remain constant at any instant during simulation if $N_{i,j}$ is fixed. $\theta_{i,n,l}$ is a uniformly

DOI: 10.1002/dac

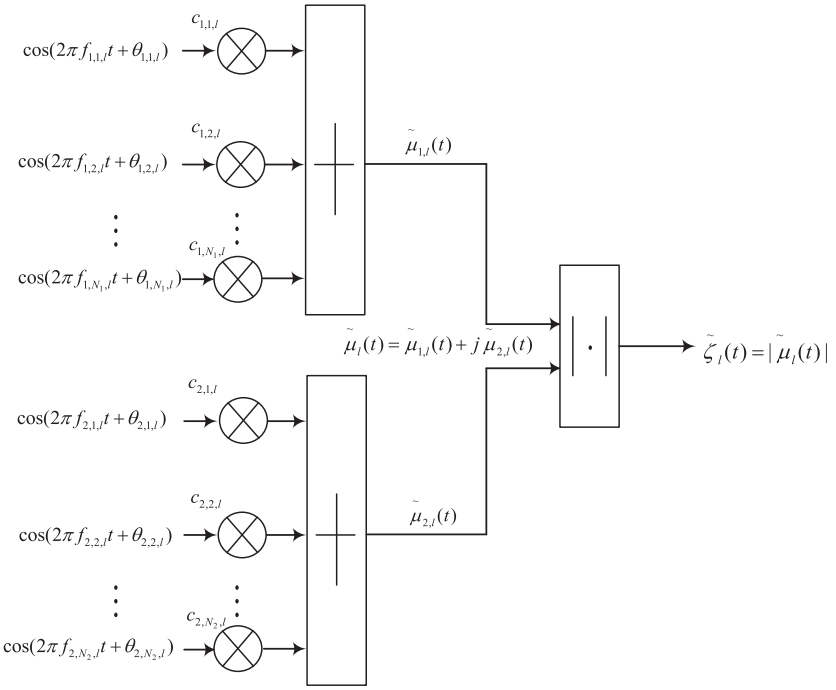

Figure 1. Structure of SOS simulator for Rayleigh channel

distributed random value over $(0, 2\pi]$. Once randomly generated at the beginning, $\theta_{i,n,l}$ keeps constant throughout the whole simulation. The structure of the SOS fading channel generation is plotted in Figure 1.

For deterministic process $\tilde{\mu}_{i,l}(t)$, the statistical properties can be calculated by time averaging. Specifically, we assume that time variable t is a random variable uniformly distributed within the interval $\mathbb{R}$. The major properties are given in [21].

$$\tilde{r}_{\mu_{i,l}\mu_{i,l}}(\tau)=\sum_{n=1}^{N_{i,l}}\frac{c_{i,n,l}^2}{2}\cos(2\pi f_{i,n,l}\tau) \tag{9}$$

$$\tilde{r}_{\mu_{i,k}\mu_{\lambda,l}}(\tau)=\begin{cases}\sum\limits_{n=1}^{N_{1,l}}\sum\limits_{m=1}^{N_{2,l}}\frac{c_{i,n,k}c_{\lambda,m,l}}{2}\cos(2\pi f_{i,n,k}\tau-\theta_{i,n,k}\pm\theta_{\lambda,m,l}), if\ f_{i,n,k}=\pm f_{\lambda,m,l}\\ 0, \qquad\qquad if\ f_{i,n,k}\neq\pm f_{\lambda,m,l}\end{cases} \tag{10}$$

$$\tilde{r}_{\mu_l\mu_l}(\tau)=\sum_{i=1}^{2}\tilde{r}_{\mu_{i,l}\mu_{i,l}}(\tau)+j\left[\tilde{r}_{\mu_{1,l}\mu_{2,l}}(\tau)-\tilde{r}_{\mu_{2,l}\mu_{1,l}}(\tau)\right] \tag{11}$$

In (10), the necessary and sufficient conditions to guarantee two processes $\tilde{\mu}_{i,l}(t)$ and $\tilde{\mu}_{k,\lambda}(t)$ uncorrelated are

$$f_{i,n,k}\neq\pm f_{i,n,l}\qquad k\neq l \tag{12}$$

and

$$f_{i,n,k}\neq\pm f_{\lambda,m,l}\qquad i\neq\lambda \tag{13}$$

and they hold for any $n=1,2,...,N_{i,k}$ and $m=1,2,...,N_{\lambda,l}$. Because $N_{i,k}$ and $N_{\lambda,l}$ are finite values in simulation, the performance of the SOS method could only approach but never reach

DOI: 10.1002/dac

(3)–(6). Therefore, we rely upon $L_p - norm$ to evaluate the performance of correlation function defined by

$$E_{i,l}^{(p)} = \left[\frac{1}{\tau_{\max}} \int_0^{\tau_{\max}} |r_{\mu_{i,l}\mu_{i,l}}(\tau) - \tilde{r}_{\mu_{i,l}\mu_{i,l}}(\tau)|^p d\tau \right]^{1/p} \tag{14}$$

$$E_{l}^{(p)} = \left[\frac{1}{\tau_{\max}} \int_0^{\tau_{\max}} |r_{\mu_l\mu_l}(\tau) - \tilde{r}_{\mu_l\mu_l}(\tau)|^p d\tau \right]^{1/p} \tag{15}$$

where $\tau_{\max}$ denotes an appropriate time interval $[0, \tau_{\max}]$ over which the approximation of ACF is of great interest to us. In this paper, we set $p = 2$ and the $L_p - norm$ turns to be the mean-square error.

2.3. Generalized method of exact Doppler spread ($GMEDS_q$)

On the basis of the inequality of (12) and (13), [22] proposed the GMEDS_q. In this method, Doppler coefficients and discrete Doppler frequencies are given by

$$c_{i,n,l} = \sigma_0 \sqrt{\frac{2}{N_{i,l}}} \tag{16}$$

$$\begin{aligned} f_{i,n,l} &= f_{\max} \cos(\alpha_{i,n,l}) \\ &= f_{\max} \cos\left[\frac{q\pi}{2N_{i,l}} \left(n - \frac{1}{2} \right) + \alpha_{i,0,l} \right] \end{aligned} \tag{17}$$

Here, $\alpha_{i,n,l}$ is the angle of arrival and $\alpha_{i,0,l}$ is the angle of rotation. $\forall l,\ N_{i,l} = N_i$. The quantity $q \in \{1, 2\}$ determines the range of the angle of arrival. Studies have shown that for the GMEDS_q, the quantity $\tau_{\max}$ in (14) is given by $\tau_{\max} = \frac{N_i}{2q f_{\max}}$. If $q = 1$ and $\alpha_{i,0,l} = 0$, GMEDS_q reduces to the original MEDS in [12], which can produce quasi-optimal approximation of the ACF corresponding to few channels, but not sufficiently effective in multiple uncorrelated channels, especially in the case when L is large. In [22], two special cases are introduced to compute the parameter of the $f_{i,n,l}$.

For GMEDS_1:

$$\alpha_{i,0,l} = (-1)^{i-1} \frac{\pi}{4N_i} \frac{l}{L+2}, \qquad N_1 = N_2 \tag{18}$$

For GMEDS_2:

$$\alpha_{i,0,l} = \frac{\pi}{4N_i} \frac{l-1}{L-1}, \qquad N_2 = N_1 + 1 \tag{19}$$

3. NEW COMPUTATIONAL METHOD

3.1. Analysis on generalized method of exact Doppler spread ($GMEDS_2$)

In (18), $\alpha_{i,0,l}$ is over $\left[0, \frac{\pi}{4N_i}\right]$. We conclude that $\alpha_{i,n,l}$ is bounded over interval $(0, \pi)$, because

$$\begin{aligned} &\frac{\pi}{2N_i} \leqslant \frac{\pi}{N_i} \left(n - \frac{1}{2} \right) \leqslant \pi - \frac{\pi}{2N_i} \\ \Rightarrow\ &0 < \frac{\pi}{2N_i} \leqslant \alpha_{i,n,l} \leqslant \pi - \frac{\pi}{4N_i} < \pi \end{aligned} \tag{20}$$

DOI: 10.1002/dac

Because of the property of cosine function, $\alpha_{i,n,l}$ and $\pi - \alpha_{i,n,l}$ lead to the same $f_{i,n,l}$. Thus, the inequalities in (12) and (13) can be rewritten as follows:

$$\alpha_{i,0,k} \neq \alpha_{i,0,l}, \qquad k \neq l \tag{21}$$

$$\alpha_{i,0,k} \neq \pi - \alpha_{i,0,l}, \qquad k \neq l \tag{22}$$

$$\alpha_{i,0,k} \neq \alpha_{\lambda,0,l} + \frac{\pi(2m-1)}{2N_\lambda} - \frac{\pi(2n-1)}{2N_i}, \qquad i \neq \lambda \tag{23}$$

$$\alpha_{i,0,k} \neq \pi - \alpha_{\lambda,0,l} - \frac{\pi(2m-1)}{2N_\lambda} + \frac{\pi(2n-1)}{2N_i}, \qquad i \neq \lambda \tag{24}$$

If substituting (18) into (23), we find the inequality (23) cannot be satisfied under certain conditions. Because $N_2 = N_1 + 1$, close analysis shows that if we set $m = n, i = 1, \lambda = 2$, (23) becomes

$$\alpha_{1,0,k} \neq \alpha_{2,0,l} + \frac{\pi(2m-1)}{2N_1(N_1+1)}, i \neq \lambda \tag{25}$$

Although $\alpha_{i,0,l}$ is limited to the interval $\left[0, \frac{\pi}{4N_i}\right]$, it is insufficient to keep (21)–(24) true. The $\alpha_{i,0,l}$ should be appropriately chosen to satisfy those inequalities. However, the form of (19) is not the case. In substituting (19) into (25) and setting $l = 1$, (25) turns to

$$\frac{\pi(k-1)}{4(N_1+1)(L-1)} \neq \frac{\pi(2m-1)}{2N_1(N_1+1)}, i \neq \lambda \tag{26}$$

This inequality frequently fails to stand, thus it easily becomes an equality. For example, when $N_1 = 20, \quad L = 3$,

$$\begin{aligned} f_{1,3,1} &= f_{\max} \cos\left[\frac{\pi(2\times 3-1)}{2\times 20} + \frac{\pi(1-1)}{4\times 20\times(3-1)}\right] \\ &= f_{\max}\cos\frac{\pi}{8} \end{aligned} \tag{27}$$

$$\begin{aligned} f_{2,3,2} &= f_{\max} \cos\left[\frac{\pi(2\times 3-1)}{2\times 21} + \frac{\pi(2-1)}{4\times 21\times(3-1)}\right] \\ &= f_{\max}\cos\frac{\pi}{8} = f_{1,3,1} \end{aligned} \tag{28}$$

Therefore, the closed form given in (19) is inappropriate to ensure the uncorrelatedness among L Rayleigh channels.

3.2. Computational method

To solve the uncorrelatedness mentioned in Section 3.1, we propose a new parameter computational method as

$$\alpha_{i,0,l} = \frac{\pi}{2LN_i}\left(l - \frac{1}{2}\right) \tag{29}$$

where $l = 1, 2, ..., L$; $N_2 = N_1 + 1$. The $\alpha_{i,n,l}$ could be represented as

$$\alpha_{i,n,l} = \frac{(2n-1)}{2N_i}\pi + \frac{(2l-1)}{4LN_i}\pi = \frac{2L(2n-1)+(2l-1)}{4LN_i}\pi \tag{30}$$

where $n = 1, 2, ..., N_i$ and $l = 1, 2, ..., L$. For fixed i, n, $\{\alpha_{i,n,l}\}_{l=1}^{L}$ represents a set of L angles between $\frac{2L\times(2n-1)+1}{4LN_i}\pi$ and $\frac{2L\times 2n-1}{4LN_i}\pi$ with the same interval $\frac{1}{2LN_i}\pi$. We note that $\alpha_{i,n,l}$ is limited

DOI: 10.1002/dac

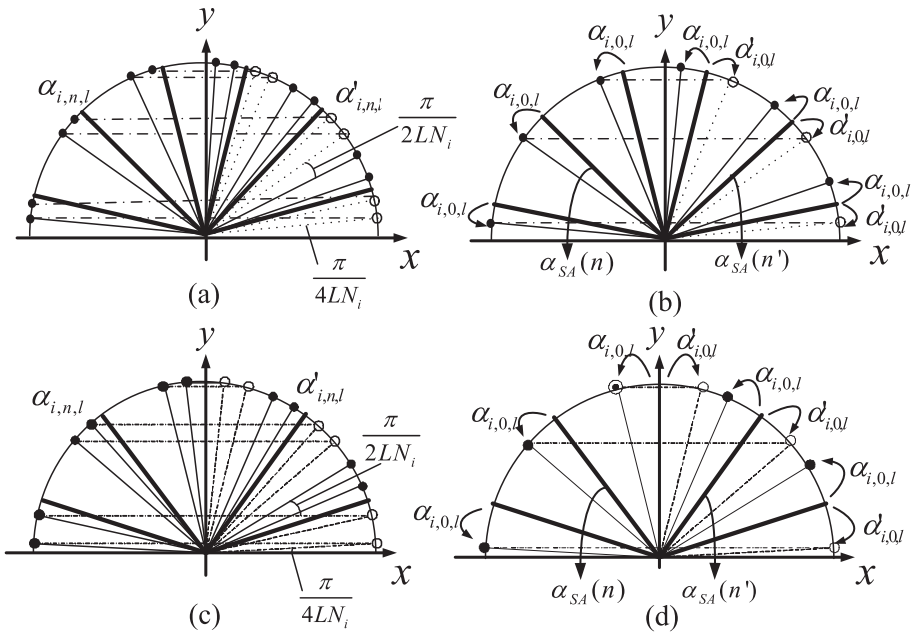

Figure 2. The projection from $\alpha_{i,n,l}$ to $\alpha'_{i,n,l}$ ('•' represents the original angles $\alpha_{i,n,l}$. '○' represents the mapped angles $\alpha'_{i,n,l}$). In (a) and (b) $N_i = 6$. In (c) and (d), $N_i = 5$.

to $(0, \pi)$, where cosine function is not monotone. To simplify the analysis, we project $\alpha_{i,n,l}$ over $\left(\frac{\pi}{2}, \pi\right)$ to $\alpha'_{i,n,l}$ over $\left(0, \frac{\pi}{2}\right)$ while keeping $|\cos\alpha_{i,n,l}| = |\cos\alpha'_{i,n,l}|$, i.e., $\alpha'_{i,n,l} = \pi - \alpha_{i,n,l}$. We use a half-ring model to illustrate such projection in Figure 2.

On the basis of (30), the $\alpha'_{i,n,l}$ can be represented as

$$\alpha'_{i,n,l} = \pi - \alpha_{i,n,l} = \frac{(2n-1)}{2N_i}\pi - \frac{(2l-1)}{4LN_i}\pi = \frac{2L(2n-1)-(2l-1)}{4LN_i}\pi \tag{31}$$

where $n = 1, 2, ..., \left\lfloor \frac{N_i}{2} \right\rfloor$ and $l = 1, 2, ..., L$. $\left\lfloor \frac{N_i}{2} \right\rfloor$ denotes the biggest integer smaller than $\frac{N_i}{2}$.

We further combine $\{\alpha_{i,n,l}\}$ and $\{\alpha'_{i,n,l}\}$ over $\left(0, \frac{\pi}{2}\right]$ into a new set $\{\overline{\alpha}_{i,n,l}\}_{l=1}^{L}$. For any n, $\{\overline{\alpha}_{i,n,l}\}_{l=1}^{L}$ represents a set of L angles between $\frac{2L(2n-2)+1}{4LN_i}\pi$ and $\frac{2L(2n-1)-1}{4LN_i}\pi$ with interval $\frac{1}{2LN_i}\pi$. We thus define that

$$\bar{\alpha}_{i,n'} = \pi\frac{(2n'-1)}{4LN_i} \tag{32}$$

Here, $n' = 1, 2, ..., LN_i$. Because all $\bar{\alpha}_{i,n'}$ are evenly distributed in $\left(0, \frac{\pi}{2}\right]$, we can prove that our method guarantees the uncorrelatedness of multiple fading channels.

Proof

Let $N_2 = N_1 + 1$. Suppose the kth channel is correlated to the lth channel, we have

$$\begin{aligned} &|f_{1,n,k}| = |f_{2,m,l}| \Leftrightarrow \bar{\alpha}_{1,n'} = \bar{\alpha}_{2,m'} \\ &\Leftrightarrow \frac{\pi}{2}\frac{(2n'-1)}{4KN_1} = \frac{\pi}{2}\frac{(2m'-1)}{4KN_2} \Leftrightarrow \frac{(2n'-1)}{N_1} = \frac{(2m'-1)}{N_1+1} \end{aligned} \tag{33}$$

□

Equation (33) never holds, because an odd number divided by an odd number never equals to an odd number divided by an even number.

DOI: 10.1002/dac

4. NEW DESIGN METHOD

4.1. Angle set division

We divide the angle set $\{\alpha_{i,n,l}\}_{n=1,l=1}^{N_i,L}$ into two subsets, A and $\bar{A}$. Subset A includes all angles over $\left(0, \frac{\pi}{2}\right]$ and $\bar{A}$ includes all angles over $\left[\frac{\pi}{2}, \pi\right)$. To illustrate the relationship between the two subsets, we define the angle $\frac{\pi}{N_i}\left(n-\frac{1}{2}\right)$ as standard angles (SA), $\alpha_{\mathrm{SA}}(n)$. Similar to Section 3, we project the angles in $\bar{A}$ to angles interval over $\left(0, \frac{\pi}{2}\right]$ while keeping $|\cos\alpha_{i,n,l}| = |\cos\alpha'_{i,n,l}|$. We denote the projected angles as $\bar{A}' = \{\alpha'_{i,n,l}\}_{n=1,l=1}^{N_i,L}$. As shown in Figure 2, the angle $\alpha_{i,n,l}$ and projected $\alpha'_{i,n,l}$ are symmetric about $\alpha_{\mathrm{SA}}(n)$.

If N is even, we set $N = 2N'$. In Figure 2(b), we categorized $2N'$ angles into two groups. Each group has N' angles. Following the previously mentioned projection, we denote the original in $\left(0, \frac{\pi}{2}\right]$ as black ($'\bullet'$) and the projected angles as white ($'\circ'$).

For the standard angle with the same n, one group has $\alpha_{i,0,l}$ deviation and the other group has $-\alpha_{i,0,l}$.

We then investigate the effect of each subset on the error function in Figure 3. The error function is approximately symmetrical, that is, $E^2(\alpha_{i,0,l}) \approx E^2(-\alpha_{i,0,l})$. Although altering the $\alpha_{i,0,l}$ from zero augments the error, the error is always varying in two opposite directions. That is, the two groups can compensate each other to achieve a reduced total error. As shown earlier, $f_{i,n,l}$, which is determined by $\alpha_{i,0,l} \in \left(0, \frac{\pi}{4N_i}\right)$, is smaller than that determined by $\alpha_{i,0,l} = 0$. Similarly, $f_{i,n,l}$ determined by $\alpha_{i,0,l} \in \left(-\frac{\pi}{4N_i}, 0\right)$ is always larger than the $f_{i,n,l}$ determined by $\alpha_{i,0,l} = 0$. This means non-positive error for $\alpha_{i,0,1} > 0$ whereas non-negative error for $\alpha_{i,0,1} < 0$. Consequently, if we combine the case with both $\alpha_{i,0,1} > 0$ and $\alpha_{i,0,1} < 0$, the two subsets will compensate each other in approximating the reference model.

If N is odd, it can be expressed as $N = 2N' - 1$. We set the angles as follows.

$$f_{i,n} = f_{\max}\cos\left[\frac{\pi}{2N_i{}' - 1}\left(n - \frac{1}{2}\right) + \alpha_{i,0}\right] \quad n = 1, 2, ..., N_i \tag{34}$$

$$c_{i,n} = \begin{cases} \sqrt{\frac{1}{N_i{}' - 1/2}} & , n = 1, 2, ..., N_i - 1 \\ \sqrt{\frac{1}{2N'_i - 1}} & , n = N_i \end{cases} \tag{35}$$

We now prove that the new $2N' - 1$ set is equivalent to the original scheme in our computational method.

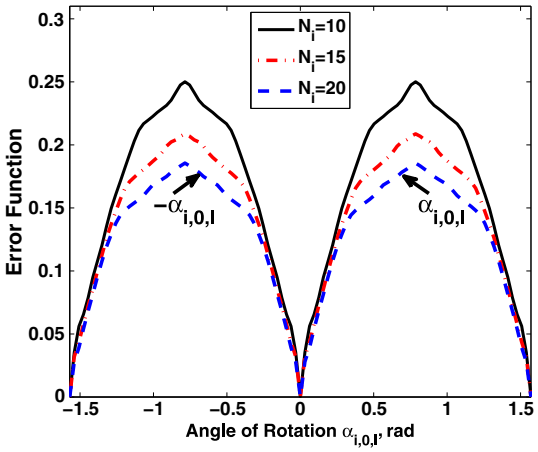

Figure 3. The error function of (14) as a function of $\alpha_{i,0,l}$.

DOI: 10.1002/dac

Proof
When $\alpha_{i,0,l}$ =0

$$\begin{aligned} f_{i,n,l} &= f_{\max}\cos(\alpha_{i,n,l}) \\ &= f_{\max}\cos\left[\frac{\pi}{N_i}\left(n-\frac{1}{2}\right)\right] \quad n=1,2,...,N_i \end{aligned} \tag{36}$$

□

There are $N'-1$ pairs of $\alpha_{i,n,l}$ and a single $\alpha_{i,n,l}=\frac{\pi}{2}$ for $n=\left\lfloor\frac{N_i}{2}\right\rfloor+1$. Each pair has the same $|f_{i,n,l}|$. For the same value of $f_{i,n,l}$, the $c_{i,n}$ for each n can be added up in the way of $c_{i,n,l}{}' = \sqrt{c_{i,m,l}{}^2 + c_{i,n,l}{}^2}$, where m and n have the same value of $|f_{i,n,l}|$. After recalculating the $c_{i,n,l}{}', n=1,2,....$ The expression $c_{i,n,l}{}'$ is equal to (35).

Therefore, the N_i angles, either odd or even, can be divided into two groups and ensure a compensating mechanism to reduce the total error of $\tilde{r}_{\mu_{1,l}\mu_{1,l}}(\tau)$.

4.2. Design method based on set partition

Inspired by the angle set division previously mentioned, we propose a new design method. Below, we first discuss the case of $N_i = 2N_i{}'$.

The ACF of $\tilde{r}_{\mu_{2,l}\mu_{2,l}}(\tau)$ can be expressed as (we force all $\sigma_0^2=1$)

$$\begin{aligned} \tilde{r}_{\mu_{i,l}\mu_{i,l}}(\tau) &= \sum_{n=1}^{N_i}\frac{c_{i,n,l}^2}{2}\cos(2\pi f_{i,n,l}\tau) = \frac{1}{N_i}\sum_{n=1}^{N_i}\cos(2\pi f_{i,n,l}\tau) \\ &= \frac{1}{2N_i{}'}\left[\sum_{n=1}^{N_i{}'}\cos(2\pi f_{i,n,l}\tau)+\sum_{n=N_i{}'+1}^{2N_i{}'}\cos(2\pi f_{i,n,l}\tau)\right] \\ &= \frac{1}{2}\left[\frac{1}{N_i{}'}\sum_{n=1}^{N_i{}'}\cos(2\pi f_{i,n,l}\tau)+\frac{1}{N_i{}'}\sum_{n=1}^{N_i{}'}\cos(2\pi f_{i,n,l}{}'\tau)\right] \\ &= \frac{1}{2}\left[\tilde{r}^{(1)}_{\mu_{i,l}\mu_{i,l}}(\tau)+\tilde{r}^{(2)}_{\mu_{i,l}\mu_{i,l}}(\tau)\right] = \bar{r}_{\mu_{i,l}\mu_{i,l}}(\tau) \end{aligned} \tag{37}$$

where $\tilde{r}^{(1)}_{\mu_{i,l}\mu_{i,l}}(\tau)$ and $\tilde{r}^{(2)}_{\mu_{i,l}\mu_{i,l}}(\tau)$ denote the ACF of each subset of angles with deviation of $\alpha_{i,n,l}$ and $-\alpha_{i,n,l}$.

$$\alpha^{(k)}_{i,n,l} = \frac{\pi}{N_i}\left(n-\frac{1}{2}\right)+(-1)^{k-1}\frac{\pi}{2LN_i}\left(l-\frac{1}{2}\right) \tag{38}$$

Because each group of component is uncorrelated to another, for the same n,

$$\alpha^{(1)}_{i,n,l}-\alpha^{(2)}_{i,n,l} = 2\alpha_{i,0,l} = \frac{\pi}{LN_i}\left(l-\frac{1}{2}\right) \tag{39}$$

On the basis of the division, there is no need to simulate all $2N'$ scatters simultaneously. Instead, we can alternatively simulate the two mutually uncorrelated deterministic processes with reduced complexity. In practice, it is recommended to simulate the two deterministic processes successively by computing from time to time, for example, using $\alpha^{(1)}_{i,n,l}$ and $\alpha^{(2)}_{i,n,l}$ for every 1000 samples in a period. From (37), the sample mean ACF $\bar{r}_{\mu_{i,l}\mu_{i,l}}(\tau)$ equals $\tilde{r}_{\mu_{i,l}\mu_{i,l}}(\tau)$. We can thereby replace $\tilde{r}_{\mu_{i,l}\mu_{i,l}}(\tau)$ in (14) and (15) by $\bar{r}_{\mu_{i,l}\mu_{i,l}}(\tau)$ to check the error function. Moreover, when $N_i \to +\infty$ it can be shown that $\bar{r}_{\mu_{i,l}\mu_{i,l}}(\tau) \to r_{\mu_{i,l}\mu_{i,l}}(\tau)$.

Similarly, when $N_i = 2N_i{}'-1$, two sets of angles in (34) and (35) can be applied for the simulation successively. The mean ACF $\bar{r}_{\mu_{i,l}\mu_{i,l}}(\tau)$ is equal to $\tilde{r}_{\mu_{i,l}\mu_{i,l}}(\tau)$ as well. Moreover, because all sets consist of $N_i{}'$ scatters, it is unnecessary to simulate it for $N_i = 2N_i{}'-1$ sinusoid scatters.

DOI: 10.1002/dac

We conclude that the new design method is able to reduce the complexity by 50%. Thus, it is an efficient way to simulate L mutually uncorrelated Rayleigh fading channels.

5. MULTIPLE CORRELATED FADING CHANNELS

Because of insufficient frequency separation in frequency diversity system and the restricted antenna spacing in space diversity systems, generation of multiple correlated fading channels is needed to evaluate the performance of those communication systems. In this section, we extend our fading channels modeling to multiple correlated cases with known covariance matrix. Specifically, we employ matrix manipulation to generate correlated channels.

5.1. Linear transform for generating correlated channels

With the new proposed method, we generate L correlated Rayleigh fading channels as $\zeta_l(t)(l = 1, 2, ...L)$. In particular, we apply linear transform to the existing uncorrelated Gaussian process $\mu_l(t)(l = 1, 2, ...L)$. The transform can be written as

$$Y = CU \tag{40}$$

where $Y = [y_1(t) \quad y_2(t) \quad \cdots \quad y_L(t)]^T$; $U = [\mu_1(t) \quad \mu_2(t) \quad \cdots \quad \mu_L(t)]^T$ and

$$C = \begin{bmatrix} c_{11} & c_{12} & \cdots & c_{1L} \\ c_{21} & c_{22} & \cdots & c_{2L} \\ \vdots & \vdots & \ddots & \vdots \\ c_{L1} & c_{L2} & \cdots & c_{LL} \end{bmatrix} \tag{41}$$

is called the coloring matrix.

Obviously, $\zeta_l(t) = |y_l(t)|$ follows Rayleigh distribution. The matrix C is determined by the correlation matrix W defined as

$$W = \begin{bmatrix} \rho_{11} & \rho_{12} & \cdots & \rho_{1L} \\ \rho_{21} & \rho_{22} & \cdots & \rho_{2L} \\ \vdots & \vdots & \ddots & \vdots \\ \rho_{L1} & \rho_{L2} & \cdots & \rho_{LL} \end{bmatrix} \tag{42}$$

where $\rho_{l\lambda} = \frac{r_{y_l y_\lambda}(\tau)}{\sqrt{r_{y_l y_l}(\tau) r_{y_\lambda y_\lambda}(\tau)}}|_{\tau=0}$. ρ is determined by features of communication channels, such as the frequency separation, channel delay spread, maximum Doppler frequency and time delay between the arrival of envelopes for two different channels.

The relation between W and C can be expressed as follows:

$$W = CC^H \tag{43}$$

From (43), the issue of determining the coloring matrix C can be turned into an issue of finding out matrix W, which can be uniquely determined by the feature of the channels.

5.2. Algorithm description

Our correlated Rayleigh fading channel generation comprised of two parts: (i) multiple channel correlation estimation and (ii) construction of multiple uncorrelated Gaussian process. On the basis of the measurements from real fading channels, we establish the covariance between the existing fading channels. As discussed in the previous section, the in-phase and quadrature component of $\mu_l(t)$ in (1) are both uncorrelated Gaussian processes; we then generate channels that are always correlated in an efficient manner.

DOI: 10.1002/dac

The algorithm requires two inputs: (i) channel measurements and (ii) system parameters. Channel measurements include frequency separation, channel delay spread, the maximum Doppler frequency and the time delay between the arrival of different channels. System parameters consist of $f_{\max}$, σ_0, N_i and L. The detailed steps are described as follows:

Step 1: Determining correlation coefficient. Specify the desired correlation matrix W. Here, we use the covariance between nth channel and lth channels. The covariance is determined by [9]:

$$u_{1nl} = \frac{\sigma_x^2 J_0(2\pi f_m \tau_{nl})}{2\left(1 + k_{nl}^2\right)} \tag{44}$$

$$u_{2nl} = -k_{nl} u_{1nl} \tag{45}$$

where $k_{nl} = 2\pi(\Delta f_{nl}\sigma)$. Δf_{nl} is the frequency separation between envelopes n and l, σ is the channels delay spread. f_m is the maximum Doppler offset; σ_x^2 is the desired power of envelope and τ_{nl} is the time delay between the arrival of nth envelope and lth envelope. The covariance matrix can be uniquely specified, with the off-diagonal elements equal to $2u_{1nl} - 2ju_{2nl}$ and the diagonal elements equal to σ_x^2. On the basis of the covariance matrix, we can further determine the correlation coefficient ρ and matrix W based on their definitions.

Step 2: Determining coloring matrix. First, factorize $W = U\Lambda U^H$. The columns of U should include a complete set of orthogonal eigenvectors, and $\Lambda = \mathrm{diag}(\lambda_1, \lambda_2, ..., \lambda_N)$. If $\lambda_i > 0\ \forall\lambda_i$, the matrix W is a positive definite matrix. We can directly obtain the low triangular matrix (43) by performing Cholesky decomposition (43).

Otherwise, compute matrix $\hat{\Lambda} = \mathrm{diag}\left(\hat{\lambda}_1, \hat{\lambda}_2, ..., \hat{\lambda}_N\right)$ where $\hat{\lambda}_i = \lambda_i$ if $\lambda_i > 0$. Then, we calculate the $\hat{W} = U\hat{\Lambda}U^H$. Because all eigenvalues of $\hat{W}$ are positive, the $\hat{W}$ is a positive definite matrix. We can thereby perform Cholesky decomposition (43).

Step 3: Uncorrelated channel generation. Generate L uncorrelated complex Gaussian fading channels $\mu_l(t)(l = 1, 2, ...L)$. On the basis of the predefined parameters such as $f_{\max}$, σ_0, N_i and L, we utilize the new computational method in Section 3 to ensure the uncorrelatedness among each fading channel. The design method mentioned in Section 4 is also employed to reduce the complexity of multiple fading channel generation.

Step 4: Correlated channels generation. Obtain L correlated complex Gaussian fading channels $y_l(t)(l = 1, 2, L)$ by applying linear transform (40) on $\mu_l(t)(l = 1, 2, ...L)$. The envelopes of $\zeta_l(t) = |y_l(t)|$, $l = 1, 2, ..., L$, are multiple correlated Rayleigh fading channels. $\zeta_l(t)$ is the final output of our algorithm.

6. PERFORMANCE EVALUATION

In this section, we conduct performance evaluation on the proposed method in Sections 3–5. All simulation results presented here are collected by using $f_{\max} = 91Hz$, $N_1 = 30$, $N_2 = 31$, $L = 3$, $T_s = 10^{-4}$s, unless otherwise stated.

6.1. Comparison with reference model

The simulation results of autocorrelations of the quadrature component and of the complex envelopes are presented in Figure 4. In Figure 4(a), we plot three different $\tilde{r}_{\mu_{1,l}\mu_{1,l}}(\tau)$ curves for $\alpha_{i,0,l}$ based on different selections of l. The reference model is calculated by using (3) and (5). Figure 4(b) depicts the complex envelop of $\tilde{r}_{\mu_l\mu_l}(\tau)$. We observe that all three fading channels have an accurate approximation to the reference model.

We investigate the PDF of our generated fading channels in Figure 5. We include more than 10^6 samples in simulation. Visibly, the PDF agrees well with the reference model described by (2).

DOI: 10.1002/dac

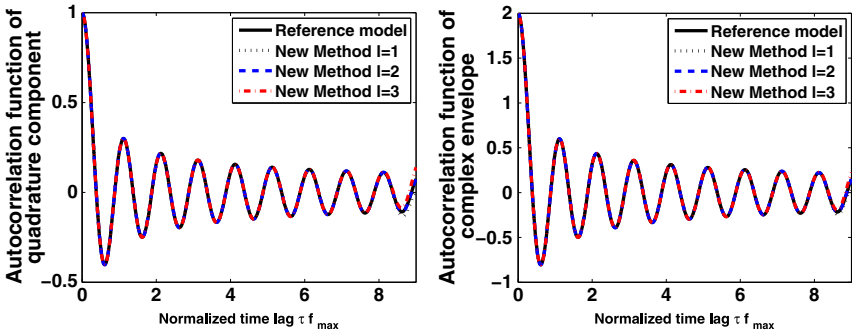

(a) Quadrature component (b) Complex envelope

Figure 4. The auto-correlation functions of the proposed method and the reference model when $l = 1, 2, 3$.

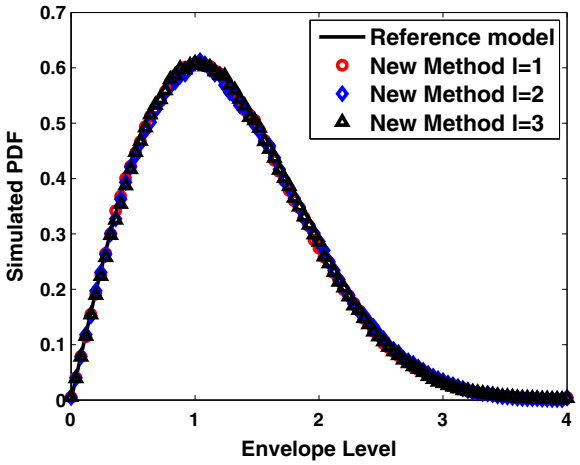

Figure 5. The envelope PDFs of the Rayleigh model and the simulation model by using $l = 1, 2, 3$.

6.2. *Comparison with existing method*

To illustrate how our method outperforms other methods in fitting reference model, we consider the square error:

$$e_2(\tau) = \left|\bar{r}_{\mu_{i,k}\mu_{i,k}}(\tau) - r_{\mu_{i,k}\mu_{i,k}}(\tau)\right|^2 \tag{46}$$

where $r_{\mu_{i,k}\mu_{i,k}}(\tau)$ is defined in (3). Figure 6 shows $e_2(\tau)$ in in-phase component and comparisons with GMEDS_q [‡] in [22] and our proposed method. When $N_1 = 30$, the new method outperforms GMEDS_1 (the number of sinusoids is N_1 or $\frac{N_i}{2}$) over $\left[0, \frac{Ni}{4f_{\max}}\right]$.

Studies into the error function (14) of envelope in in-phase component lend support to the observation that our new method outperforms GMEDS_1. Error function study shows that in GMEDS_1, when $N_1 = 15$ and $N_1 = 30$, the respective value of E_2 in inphase/quadrature components are $1.26 \times 10^{-2}/1.26 \times 10^{-2}$ and $4.3 \times 10^{-3}/4.3 \times 10^{-3}$; whereas in our new model, when $N_1 = 20$, the value of E_2 is $2.465 \times 10^{-5}/1.5277 \times 10^{-5}$.

[‡]Because the GMEDS_2 method suffers the correlation issue mentioned in Section 3, we only evaluate the performance of GMEDS_1 in this section.

DOI: 10.1002/dac

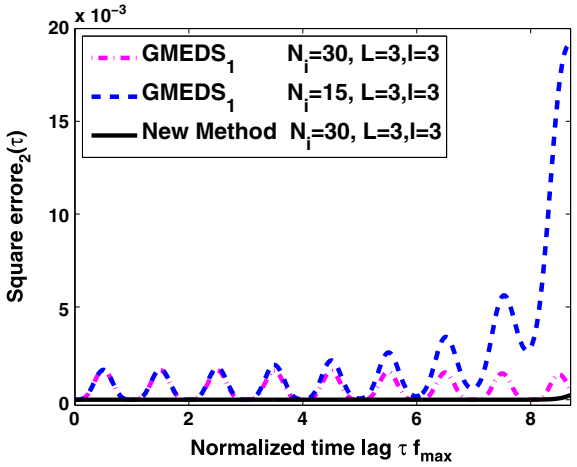

Figure 6. The square error $e_2(\tau)$ for GMEDS$_1$ and new method.

Table I. Upper limit $\hat{c}_{\mu_{i,k}\mu_{\lambda,l}}$ of the correlation coefficient of $\tilde{\mu}_{i,k}(t)$ and $\tilde{\mu}_{\lambda,l}(t)$.

$\hat{c}_{\mu_{i,k}\mu_{\lambda,l}}$	GMEDS$_1$	New method
$\hat{c}_{\mu_{1,1}\mu_{1,2}}$	$1.0968s/T$	$-0.0159s/T$
$\hat{c}_{\mu_{1,1}\mu_{1,3}}$	$0.5231s/T$	$-0.0079s/T$
$\hat{c}_{\mu_{1,2}\mu_{1,3}}$	$1.0396s/T$	$-0.1192s/T$
$\hat{c}_{\mu_{2,1}\mu_{2,2}}$	$-1.3272s/T$	$-0.0170s/T$
$\hat{c}_{\mu_{2,1}\mu_{2,3}}$	$-0.6521s/T$	$-0.0085s/T$
$\hat{c}_{\mu_{2,2}\mu_{2,3}}$	$-1.5928s/T$	$-0.1272s/T$
$\hat{c}_{\mu_{1,1}\mu_{2,1}}$	$-0.4919s/T$	$-0.4038s/T$

To compare the decorrelation rate of GMEDS$_1$ with that of the new method, we use the upper limit of correlation coefficient of $\tilde{\mu}_{i,k}(t)$ and $\tilde{\mu}_{\lambda,l}(t)$ under limited time constraints, which is defined in [22] as

$$\hat{c}_{\mu_{i,k}\mu_{\lambda,l}} = \frac{1}{\pi T\sqrt{N_i N_\lambda}} \sum_{n=1}^{N_i} \sum_{m=1}^{N_\lambda} \frac{f_{i,n,k}}{f_{i,n,k}^2 - f_{\lambda,m,l}^2} \tag{47}$$

The smaller the upper limit is, the faster the decorrelation rate is. As shown in Table I, our new method decorrelates much faster than GMEDS$_1$, a model that decorrelates faster than MMEDS [30] at the order of five [22]. Thus, we conclude that our method outperforms both GMEDS$_1$ and MMEDS.

Compared with the deterministic model in [17], the ACF of the proposed model fits the reference model better. Using the method in [17], we obtain an error of $J_4(\omega_m\tau)$ in in-phase component and $-J_4(\omega_m\tau)$ in quadrature component, even when $N_i \to +\infty$. In our method, there is no such error when $N_i \to +\infty$.

6.3. *Evaluation on complexity*

To examine the complexity of our system, we evaluate the expenditure and simulation speed for our new system and compare it with that of the previous work. We obtain our simulation result by replacing the continuous-time variable t by kT_s in Figure 1. We assume that the set-up phase has been already completed, so that our investigation is restricted to the computation expenditure required for the generation of the channel output sequence.

DOI: 10.1002/dac

Table II. Number of operations required for the computation of Rayleigh fading channels, $N_1 = 30$, $N_2 = 31$, $L = 9$.

	Number of multiplication	Number of addition	Number of trig. operations
GMEDS_1 or MMEDS	567	558	549
New method	297	288	279

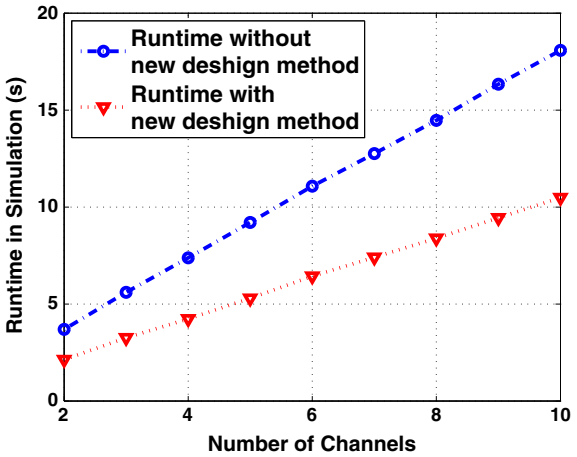

Figure 7. Runtime of our method in simulation.

Table III. The parameters for simulation correlated channels.

Parameter	Definition	Value
Δf	Frequency separation	312.5 kHz
f_m	Maximum Doppler offset	50 Hz
σ	Channel delay spread	0.1 μs
$\tau_{12}, \tau_{23}, \tau_{13}$	Time delay between channels between i and j, where $i, j = 1,2,3$, and $i \neq j$	1.1, 3.0, and 4.1 ms
σ_x	Desired power for each channel	1 W

Table II lists the number of required operations to generate nine Rayleigh fading channels. It shows the necessary operations for computing one sample of Rayleigh fading waveform at an instant k. By comparing with GMEDS_1, our new method uses only half of the original computational cost in multiplication, addition and trigonometric operations. Such reduction in complexity can save the amount of runtime in simulation and can further trim down the expenditure in hardware implementation. Figure 7 shows the total runtime with and without the design method mentioned in Section 4. We observe that the new design method is able to significantly reduce the time taken to generate channels.

6.4. Evaluation on correlated channels

To evaluate the performance of multiple correlated channels, we simulate our fading channel by setting the parameters as in Table III. Figure 8 plots the simulated fading envelopes for three correlated fading channels in the time interval of $(0, 0.1]$. The waveforms for uncorrelated fading channels (with the same $f_{\max}$, σ_0, N_i and L in computational method) are depicted for comparison. In Figure 8(a), we found that the three envelopes are related at different levels. The waveforms with $l = 1$ and $l = 2$ are highly correlated whereas the envelopes of $l = 1$ and $l = 3$ are less similar. In contrast, the three waveforms shown in Figure 8(b) are mutually uncorrelated to each other.

DOI: 10.1002/dac

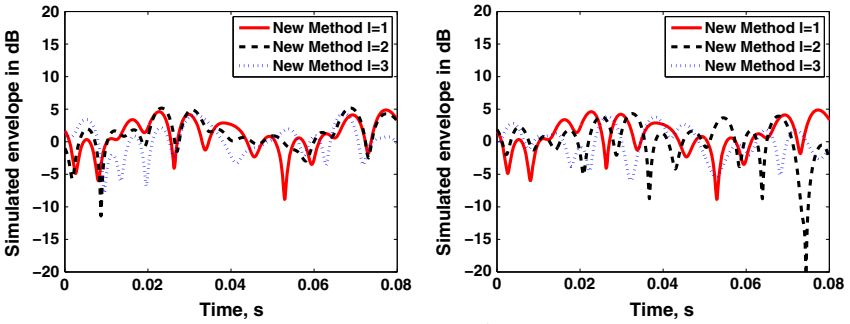

(a) The waveform of three correlated channels (b) The waveform of three uncorrelated channels

Figure 8. Simulated (a) uncorrelated and (b) correlated Rayleigh fading waveforms ($l = 1, 2, 3$) by using new method.

7. CONCLUSION

In this paper, we present a new model to generate multiple pure Rayleigh fading channels, either uncorrelated or correlated. To generate uncorrelated channels, we propose a parameter computational method and a system design method. The computational method generates uncorrelated channels with high accuracy, and the system design method reduces the computational cost. Then, we apply linear transformation by manipulating matrix to generate correlated channels using the same system. Extensive experimental results demonstrate that our proposed model is able to generate multiple fully uncorrelated Rayleigh fading channels, regardless of experimental conditions; also, computational cost is reduced without sacrificing the system performance. Results also indicate that our system is able to generate fully correlated fading channels, if needed in some scenarios.

REFERENCES

1. Gutérrez C, Matthias Pätzold M. On the correlation and ergodic properties of the squared envelope of SOC Rayleigh fading channel simulators. *Wireless Personal Communications* 2013; **68**(3):963-979.
2. Varzakas P. Average channel capacity for Rayleigh fading spread spectrum MIMO systems: research articles. *International Journal of Communications Systems* 2006; **19**(10):1081–1087.
3. Chandra A, Bose C, Bose MK. Unified BER and optimum threshold analysis of binary modulations in simple and cascaded Rayleigh fading channels with switched combining. *International Journal of Communications Systems* 2011; **24**(2):153–167.
4. Varzakas P. Optimum processing gain for a hybrid direct sequence/slow frequency hopping code division multiple access cellular system over Rayleigh fading channels: the direct sequence/slow frequency hopping code division multiple access case. *International Journal of Communication Systems* 2012; **25**:1034–1043.
5. Cvetkovic AM, Djordjevic GT, Stefanovic MC. Performance analysis of dual switched diversity over correlated Weibull fading channels with co-channel interference. *International Journal of Communications Systems* 2011; **24**(9):1183–1195.
6. Rice SO. Mathematical analysis of random noise. *Bell System Technical Journal* 1944; **23**:282–332.
7. Rice SO. Mathematical analysis of random noise. *Bell System Technical Journal* 1945; **24**:46–156.
8. Clarke RH. A statistical theory of mobile-radio reception. *Bell System Technical Journal* 1968; **47**:957–1000.
9. Jakes WC (ed.). *Microwave Mobile Communications*. Wiley: New York, 1994.
10. Pop MF, Beaulieu NC. Limitations of sum-of-sinusoids fading channel simulators. *IEEE Transactions on Communications* 2001; **49**:699–708.
11. Li Y, Huang X. The simulation of independent Rayleigh faders. *IEEE Transactions on Communications* 2002; **50**(9):1503–1514.
12. Pätzold M. *Mobile Fading Channels*. John Wiley & Sons, Inc.: New York, NY, USA, 2003.
13. Zheng YR, Xiao C. Improved models for the generation of multiple uncorrelated Rayleigh fading waveforms. *IEEE Communications Letters* 2002; **6**(6):256–258.
14. Zheng YR, Xiao C. Simulation models with correct statistical properties for Rayleigh fading channels. *IEEE Transactions on Communications* 2003; **51**(6):920–928.
15. Patel CS, Stüber GL, Pratt TG. Comparative analysis of statistical models for the simulation of Rayleigh faded cellular channels. *IEEE Transactions on Communications* 2005; **53**(6):1017–1026.

DOI: 10.1002/dac

16. Xiao C, Zheng YR, Beaulieu NC. Second-order statistical properties of the WSS Jakes' fading channel simulator. *IEEE Transactions on Communications* 2002; **50**(6):888–891.
17. Zajic AG, Stüber GL. Efficient simulation of Rayleigh fading with enhanced de-correlation properties. *IEEE Transactions on Wireless Communications* 2006; **5**(7):1866–1875.
18. Alimohammad A, Fard SF, Cockburn BF, Schlegel C. An accurate and compact Rayleigh and Rician fading channel simulator. *Vehicular Technology Conference (VTC)*, Singapore, 2008; 409–413.
19. Cheng X, Wang CX, Laurenson DI, Salous S, Vasilakos AV. New deterministic and stochastic simulation models for non-isotropic scattering mobile-to-mobile Rayleigh fading channels. *Wireless Communications and Mobile Computing* 2011; **11**(7):829–842.
20. Pätzold M, Killat U, Laue F, Li Y. On the problems of Monte Carlo method based simulation models for mobile radio channels. *Proceedings of IEEE 4th International Symposium on Spread Spectrum Techniques Applications ISSSTA*, Mainz, Germany, 1996; 1214–1220.
21. Wang CX, Patzold M, Yuan D. Accurate and efficient simulation of multiple uncorrelated Rayleigh fading waveforms. *IEEE Transactions on Wireless Communications* 2007; **6**(3):833–839.
22. Pätzold M, Wang CX, Hogstad BO. Two new sum-of-sinusoids-based methods for the efficient generation of multiple uncorrelated Rayleigh fading waveforms. *IEEE Transactions on Wireless Communications* 2009; **8**(6):3122–3131.
23. Pätzold M, Hogstad BO, Kim D. A new design concept for high-performance fading channel simulators using set partitioning. *IEEE Transactions on Wireless Communications* 2007; **40**(3):267–279.
24. Gan Y, Xu Q. An improved SoS method for generating multiple uncorrelated Rayleigh fading waveforms. *IEEE Communications Letters.* 2010; **14**(7):641–643.
25. Gutierrez CA, Patzold M, Sandoval A, Delgado-Mata C. An ergodic sum-of-cisoids simulator for multiple uncorrelated Rayleigh fading channels under generalized scattering conditions. *IEEE Transactions on Vehicular Technology* 2012; **61**(5):2375–2382.
26. Alimohammad A, Fard SF, Cockburn BF. Hardware implementation of Rayleigh and Ricean variate generators. *IEEE Transactions on Very Large Scale Integration (VLSI) Systems* 2011; **19**(8):1495–1499.
27. Alimohammad A, Fard SF, Cockburn BF, Schlegel C. Compact Rayleigh and Rician fading simulator based on random walk processes. *Communications, IET* 2009; **3**(8):1333–1342.
28. Ren F, Zheng YR. Hardware emulation of wideband correlated multiple-input multiple-output fading channels. *Journal of Signal Processing Systems* 2012; **66**(3):273–284.
29. Dent P, Bottomley GE, Croft T. Jakes fading model revisited. *Electronics Letters* 1993; **29**(13):1162–1163.
30. Wang C, Yuan D, Chen HH, Xu W. An improved deterministic SoS channel simulator for multiple uncorrelated Rayleigh fading channels. *IEEE Transactions on Wireless Communications* 2008; **7**(9):3307–3311.

AUTHORS' BIOGRAPHIES

Yu Gan received the BSc degree in Electronic and Information Engineering in 2007, from Nanjing University of Science and Technology. He received his ME degree in Communication and Information System in 2010, from the Institute of Electronics, Chinese Academy of Sciences. He is now a graduate student in the Charles V. Schaefer, JR. School of Engineering and Science at Stevens Institute of Technology. His research interests include digital signal processing and image processing. He has served as reviewer for several international journals.

You Wu received the ME degree in biomedical engineering in 2010, from the Institute of Biomedical Engineering at Chinese Academy of Medical Sciences. She is currently a graduate student in the Charles V. Schaefer, JR. School of Engineering and Science at Stevens Institute of Technology. Her research interests include biomedical information detection and processing.

DOI: 10.1002/dac